14th International Symposium on Particle Image Velocimetry – ISPIV 2021
August 1–5, 2021

Development of Optical Techniques for Large Volume PTV Measurements

H. Abitan[1,2*], Y. Zhang[1], S. L. Ribergård[1], J. S. Nielsen[2], C. M. Velte[1]

[1] Turbulence Research Laboratory, Technical University of Denmark, Department of Mechanical Engineering, Kgs. Lyngby, Denmark
[2] Instrument Group, Technical University of Denmark, Department of Mechanical Engineering, Kgs. Lyngby, Denmark

[*] haiab@mek.dtu.dk

Abstract

Measurements of 3D volumetric velocity fields are of great theoretical interest with numerous practical applications. These measurements are essential for studying volumetric flows that do not exhibit inherent flow symmetry, such as turbulence or vortex breakdown. In the past decade, several technological innovations facilitated the emergence of 3D-PTV techniques for measuring velocity fields at kHz rate with volumes of interest up to 10^4 cm^3 that contain $300\,\mu m$ helium-filled soap bubbles. However, when a commercial laser beam with millijoule pulse-energy is expanded and shaped to fill volumes above 10^2 cm^3 for 3D-PTV experiments with $15\,\mu m$ air filled soap bubbles, one finds that the power density of the laser source is insufficient to generate a signal image. This is because the power density of the laser beam falls inversely with respect to its cross-section area and due to the quadratic dependence of Mie-scattering on the particle diameter. Here, we report of the analysis and development of two optical techniques for extending the volume of measurement in volumetric PTV. In particular, when a volume about 10^3 cm^3 is seeded with $15\,\mu m$ air-filled soap bubbles and a laser with a pulse energy of few single mJ illuminates it. The first technique uses multi reflections between two opposing parallel mirrors. The second technique is a development of laser scanning PIV for volumetric scanning: The potential to increase the scanned volume is examined by experimenting with an acousto-optic modulator for fast scanning. Furthermore, by employing an off-axis parabolic mirror, we obtain parallel beam scanning, which increases the efficiency and quality of the scanning.

1 Introduction

In the past decade, techniques for volumetric velocimetry of fluid flows have been rapidly evolving. Brücker and Althaus (1992) developed the laser-sheet scanning-PIV technique already three decades ago. It was actually the first attempt to conduct 3D-PIV volumetric flow measurement. Three years later Brücker (1995) used laser scanning with time laps to obtain temporal 3D-PIV. Elsinga et al. (2006) reported of a volumetric PIV, which they named "tomographic PIV". In this method, images from 3-4 tilted cameras were obtained simultaneously and analysed with triangulations to calculate the location of particles. Since 2012 and till date computational capacity grew, the responsivity of CMOS detectors improved and also algorithms to calculate the velocity field from images became more efficient. In particular, the algorithm coined 'shake the box' (STB) by Schanz et al. (2016) reduced significantly the required calculations.

Recent 3D PTV methods use several cameras to acquire simultaneous images from a volume of interest that is illuminated by a laser beam or by LEDs. A survey, reported by Barros et al. (2021) shows that at sub kHz repetition rate the volume of interest is typically up to the order of 10^2 cm^3 using $1\,\mu m$ oil droplets, up to 10^4 cm^3 using $300\,\mu m$ helium filled soap bubbles, or up to about 10^3 cm^3 using $15\,\mu m$ air filled soap bubbles (henceforth 'soap bubbles'). However, for some investigations of turbulent flows, it is essential to extend further the size of the volume of interest and work at high laser repetition rate. For example, investigation of turbulence jet flow with millimetre spatial resolution requires a volume of interest about 10^3 cm^3 with $15\,\mu m$ soap bubbles as tracer particles at 4 kHz repetition rate Zhang et al. (2021).

In PTV measurements with a laser and tracer particles with a diameter larger than the laser wavelength, the image signal of a particle depends linearly on the optical intensity of the laser beam and quadratically on

the diameter of the scattering particle. Since the optical intensity depends inversely on the cross-section area of the laser beam, one finds that as the laser beam cross-section increases with volume size, the optical power density from available high-power commercial lasers (few mJ pulse energy at few kHz repetition rate) is not sufficient for generating a detectable image signal. The low signal problem becomes significantly noticeable when $15\,\mu m$ soap bubbles are used, due to four orders of magnitude drop in Mie scattering signal from $15\,\mu m$ soap bubbles, compared with $300\,\mu m$ helium-filled soap bubbles.

Here we report of the development of two optical techniques for overcoming the problem of low image signal in large volumetric 3D-PTV measurements. In particular when a $532\,nm$ laser with pulse energy of few single millijoule is illuminating $15\,\mu m$ soap bubbles tracer particles. The strategy underlining the two techniques is to shape the cross-section area of the laser beam into a collimated elliptic beam with a cross-section area that is tested to have the required power density flux for generating a detectable image from $15\,\mu m$ soap bubbles. Then, a collimated elliptic laser beam is shaped to have the required power density flux and it is used multiple times. In the first technique, the laser beam is incident onto two parallel opposing mirrors and it goes multiple reflections while filling the volume between the mirrors with sufficient optical power density. In the second technique, we examine the reuse of a laser beam by fast transverse scanning with an acousto-optic modulator. The rotated laser beam that is outgoing from the acuosto-optic crystal is reflected by an off-axis parabolic mirror to obtain parallel beam scanning over the volume. Since the scanning rate of acousto-optic modulators is larger by three orders of magnitudes compared with mechanical methods (such as galvanic mirrors), it has the potential to scan larger volumes per image frame. Our present acousto-optic scanner is far from being suitable for the final system. However, it taught us of the great potential it holds.

Figure 1.(a) is a top-view sketch of a set-up for multi-reflection between two parallel mirrors. A collimated elliptic laser beam is shaped to have the required power density flux. The laser beam is incident onto the left-hand side of the rear mirror. Then, the incident beam is reflected towards the opposing parallel front mirror and vice versa multiple times until it exits the right-hand side of the volume between the two parallel mirrors. Both mirrors are highly reflective with appropriate dimensions. The angle of incidence of the laser beam is set to optimize the filling of the volume of interest with optical power density while minimizing losses at the entrance into the volume and at the exit from the volume.

Figure 1.(b) shows a laser beam that is transmitted through an Acousto-Optic Modulator (AOM). Placing the AOM at the focal point of an off-axis parabolic mirror as is shown in Figure 1.(b) results in parallel beams scanning over a volume.

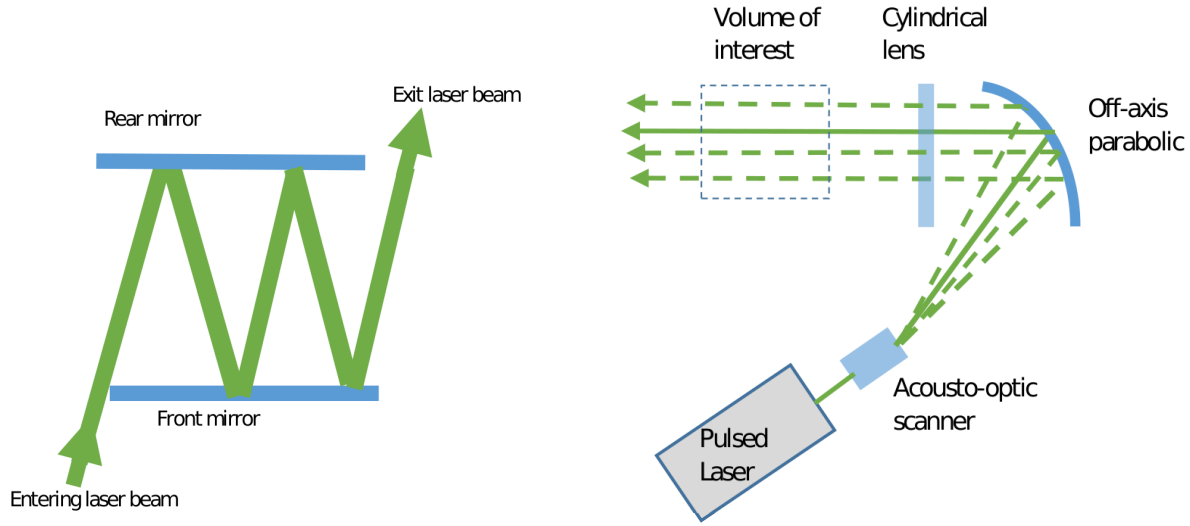

(a) The set-up for multi-reflections

(b) The set-up for acousto-optic scanning

Figure 1: Fig.1 (a) is a top-view sketch to illustrates the idea of multi-reflections. Fig.1 (b) is a top-view sketch to illustrate the idea of fast scanning with an acousto-optic modulator and an off-axis parabolic mirror.

2 Multi-Reflection

Ghaemi and Scarano (2010) reported on a method called multi-pass amplification for volumetric PIV measurements. In this method, a laser beam is reflected between two opposing mirrors that are almost parallel. The small angle between the two mirrors is set so that the incident laser beam at one edge of the mirror will propagate by reflections toward the edge at the other end of each mirror with decreasing distances between sequential reflections. The closer the laser beam progresses toward the other end of a mirror, the more dense are the reflections. The small angle between the planes of the mirrors is set so that when the beam reaches the opposite end of the mirrors, it starts to reverse its direction backward. The resulting optical power density between the two opposing mirrors is inhomogeneous. The power density is rarefied where the beam is initially incident and it is highly dens at the opposite side of the mirrors. This is not ideal for generating large scale volumes with roughly homogeneous optical density for volumetric PTV measurements. In multi-pass amplification, volumetric imaging is done at the part of the volume where the power density flux is large enough to generate a detectable image of the Mie scattering particle. In this method, the power of the laser beam is not used efficiently to generate a maximal volume with the required power energy flux.

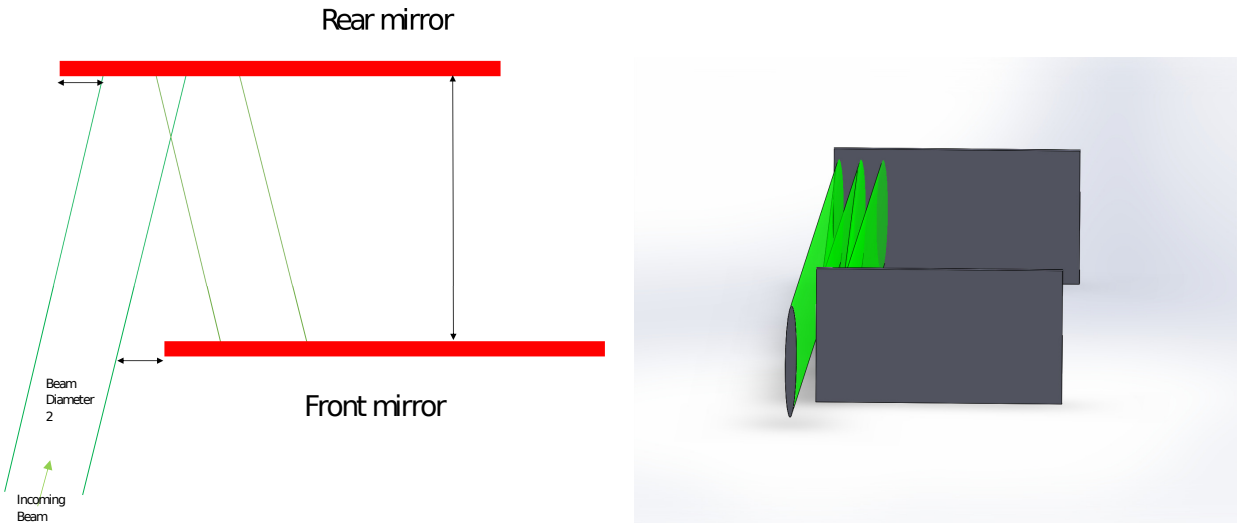

(a) Top-view sketch of multi-reflections

(b) 3D visualization of multi-reflections

Figure 2: Fig.2 (a) is a top-view sketch showing two parallel mirrors with offset. Fig.2 (b) illustrate that the laser beam has an elliptic cross-section area with noticeable dimensions compared with the rectangular mirrors

Here, we analyse and experiment with multi reflections between two parallel rectangular mirrors for volumetric 3D-PTV measurements as shown Figure 2.(a). The parallel mirrors have a slight off-set, in order to minimize the angle of incidence. The incoming laser beam is reflected from the rear mirror toward the reflective side of the front mirror and vice versa. The reflections points are equidistant. The laser beam is shaped to have an elliptic and collimated cross-section area as illustrated in Figure 2.(b). The minor and the major beam waists are set by requiring that the corresponding power density flux (i.e., the laser intensity) will generate an acceptable image signal. The required power density flux was found experimentally: a pulsed laser with an expanding Gaussian beam was transmitted through a volume containing the $15\,\mu m$ soap bubbles. A satisfactory image signal with SNR ratio of 15 (Figure 3) was generated from the soap bubbles floating in air when they where illuminated by a laser pulse with a duration of $\tau = 220\,ns$ and an energy pulse $E_p = 2.8\,mJ$ at $4kHz$ repetition rate (532 nm Blizz laser, Innolas Photonic GmbH).

The minor and major waists of the elliptical laser beam at $900\,mm$ from the laser output mirror were calculated (by the method of ABCD Gaussian beam analysis) to be $1\,mm$ and $40\,mm$, respectively . Images of the $15\,\mu m$ soap bubbles were acquired at 90° with a Phantom camera (v2640) with a $60\,mm$ lens at $1000\,mm$ working distance. The optical minification was 16.6. By using the minification with image analysis of Figure 3, we measured that the size of the major waist is close to $40\,mm$, confirming our ABCD matrix analysis for Gaussian beams.

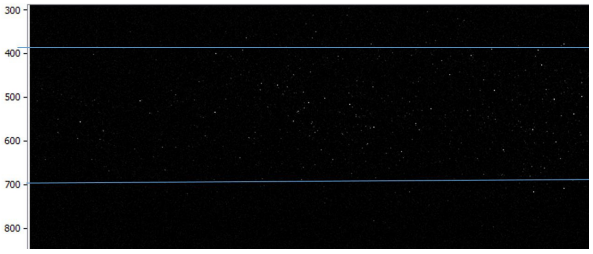

Figure 3: Image from Phantom v2640 camera when an elliptic laser beam propagates through $15\,\mu m$ soap bubbles. The image analysis confirmed our ABCD Gaussian beam analysis for the size of the major beam waist. We deduced from this image and from the laser parameters that the required optical power density flux for SNR=15 is $10\frac{[KJ]}{[s][cm^2]}$

The required power density flux is calculated by using the equation for the intensity of a pulsed laser:

$$I = \frac{E_p}{\pi\omega_a\omega_b\tau} \tag{1}$$

Inserting into Eq.1 the laser pulse-energy, pulse-duration and the laser cross-section area, the required power density flux for detecting $15\,\mu m$ soap bubbles is calculated to be $10\frac{[kJ]}{[s][cm^2]}$. In the aforementioned measurement, the camera focal lens was $f = 60\,mm$ and the working distance was $1000\,mm$. It means that if we use the same aperture diameter but we change the camera lens to $35\,mm$ and configure a working distance at $350\,mm$ (for keeping the same field of view), we would be able to use a beam cross-section with $\pi \times 5 \times 50\,mm^2$ and maintain SNR ratio of about 20.

Equipped with the required power density flux ($10\frac{[kJ]}{[s][cm^2]}$) and the corresponding cross-section area of the laser source ($\pi \times 5 \times 50\,mm^2$), the expected field of the optical power density between the two opposing mirrors can be calculated numerically. This field depends on several factors of the design: the cross-section area of the laser beam ($\pi \times 5 \times 50\,mm^2$) for $35\,mm$ lens, the angle of incidence of the laser beam, the Fresnel reflection loss, the dimensions of the reflecting mirrors compared with the cross-section area of the laser beam; and the distance between the two mirrors.

The field of the optical power density in the volume between the two opposing mirrors depends on the angle of incidence of the laser beam and on propagation and reflection losses of the beam. The propagation loss is negligible. This is due to the very small Mie scattering coefficient ($\sim 10^{-16}\frac{1}{cm^2}$). Thus the power level of the laser beam is virtually unchanged as it propagates through air with relatively low soap bubble density. However, the laser beam power drops at each reflection. The power drops due to Fresnel reflection R_F from the mirror's surface and due to the finite size of the reflecting mirrors (and the infinite extension of the elliptic Gaussian beam).

In order to fill the volume of interest with a useful optical power density, the power of the beam, just before it exits the volume of interest, needs to be above the required power density for an acceptable SNR of 10. I.e. the power density flux of the exiting beam needs to be above $10\frac{[kJ]}{[s][cm^2]}$. Figure 4 shows the drop of the predicted power of a 532 nm laser beam after consecutive Fresnel reflections from three different coatings of mirrors: aluminium, silver and dielectric. Fresnel reflection at 532 nm is $0.95, 0.975$ and 0.998 for aluminium (Thorlabs), silver (Thorlabs) and dielectric coated mirror (Laser-Optik GmbH, respectively. The calculation in Fig.4 considers only Fresnel reflection losses (the losses due to the finite size of the mirrors will be considered later below).

Examining Fig.4, we note that aluminium coated mirrors will be effective for 7 reflections. Silver coated mirrors will be effective for 27 reflections and dielectric mirrors will be effective for at least 200 reflections. At $2.8\,mJ$ pulse energy of our laser source, $350\,mm$ working distance and with minor axis $\omega_a = 5\,mm$ and major axis $\omega_b = 50\,mm$, the laser power density is about 2 times the required power density. Large volumes can be filled with such a beam if it is reflected effectively. As long as the power density of our laser beam in Fig.4 is above 0.5, the SNR will be above 10 and the signal will be detectable. Accordingly, aluminium coated mirrors could cover a volume of interest with a cross-section area of approximately $\pi \times 2.5 \times 7\,cm^2 = \sim 5.4 \times 10\,cm^2$. Silver coated mirrors could fill a volume of interest with a cross-section area

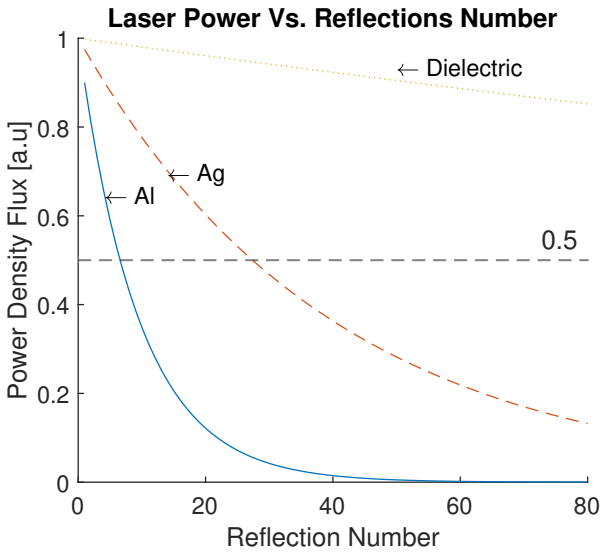

Figure 4: The power of a reflected beam vs. number of reflections. It can be seen that a dielectric mirror with 0.998 Fresnel reflectivity keeps the power of the collimated beam above the required power even after 300 reflections (The loss due to the finite size of the mirrors and the infinite size of the elliptic Gaussian beam was not consider in this calculation)

of $\pi \times 2.5 \times 27\, cm^2 =\sim 2.1 \times 10^2\, cm^2$; and dielectric mirror could fill a volume of interest with a cross-section area of $\pi \times 2.5 \times 150\, cm^2 =\sim 1.1 \times 10^3\, cm^2$. This cross-section area could be used over a length of at least $10\, cm$. It means that we could fill volumes, at least of the order of $10^4\, cm^3$.

This is a rough estimation. In order to evaluate realistically the field of the optical power density between the two parallel mirrors, we must consider the loss due to Fresnel reflection at the mirrors and evaluate numerically the loss due to the finite size of the mirrors (and the infinite extension of a Gaussian beam). In order to calculate the reflectivity of an elliptic Gaussian beam from a finite size rectangular mirror we recall from Hawkes and Latimer (1995) that the intensity of an elliptic Gaussian beam is given by:

$$I = I_0 \exp\left(-\frac{x^2}{\omega_a^2} - \frac{y^2}{\omega_b^2}\right) \tag{2}$$

The total power in such an elliptic Gaussian beam is:

$$P_{total} = I_0 \int_0^{\infty} \mathrm{e}^{-\frac{x^2}{\omega_a^2}}\,\mathrm{d}x \int_0^{\infty} \mathrm{e}^{-\frac{y^2}{\omega_b^2}}\,\mathrm{d}y \tag{3}$$

Since the rectangular mirrors has a finite size, only the part of the incident Gaussian beam that will fall on the mirror will be reflected according to Fresnel reflection law. For the purpose of clarity, let's assume that the center of the elliptic beam coincides with the center of the rectangular mirror. Then, since the beam is reflected only from the mirror, the reflected power is given by:

$$P_F = R_F \times \int_{-\frac{W}{2}}^{+\frac{W}{2}} \mathrm{e}^{\frac{-2x^2}{\omega_a^2}}\,\mathrm{d}x \int_{-\frac{H}{2}}^{+\frac{H}{2}} \mathrm{e}^{\frac{-2y^2}{\omega_b^2}}\,\mathrm{d}y \tag{4}$$

Where R_F, W and H represent Fresnel reflection, width and height of the mirrors, respectively. The effective reflected power is thus:

$$R_{eff} = \frac{P_F}{P_{total}} \tag{5}$$

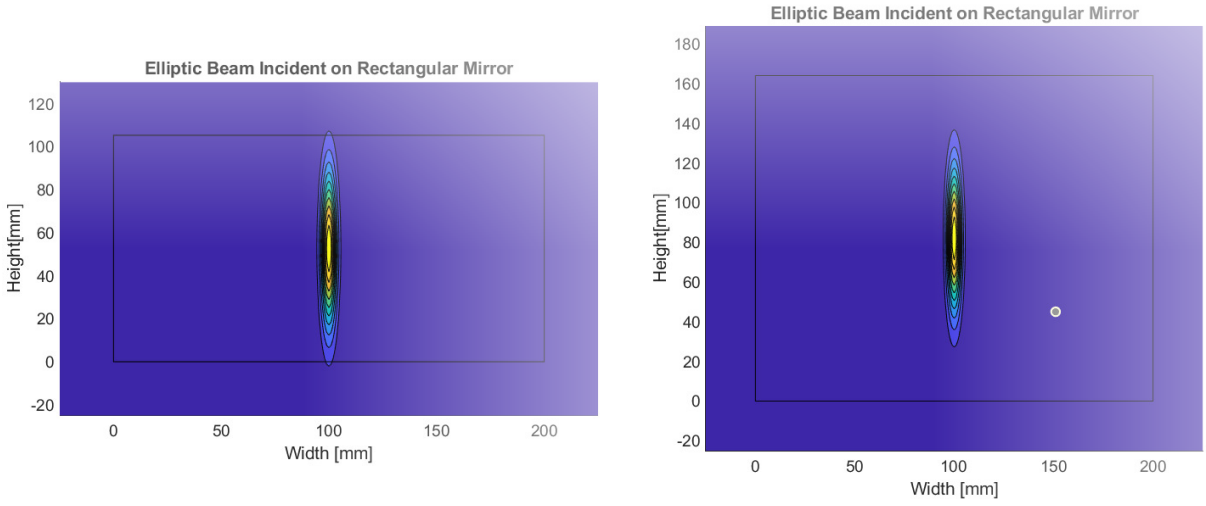

(a) (b)

Figure 5: (a) shows the cross-section of an elliptic Gaussian beam with $\omega_a = 5\,mm$ and $\omega_b = 50\,mm$ that is incident at the center of a rectangular mirror $200 \times 100\,mm$. The effective reflectivity for these mirror dimensions and beam shape is calculated numerically to be 0.963. (b) illustrates the same elliptic Gaussian beam incident on a rectangular mirror with dimensions of the mirror $200 \times 160\,mm$. The effective reflectivity is calculated to be 0.9974.

The integrals of P_{total} and P_F can be calculated analytically. $P_{total} = I_0 \frac{\pi}{2} \omega_a \omega_b$ and the integral for P_F results in expressions that involve $erf(x)$ and $erf(y)$. It turned out to be much more convenient to calculate the effective reflectivity R_{eff} by writing a Matlab program with a graphical user interface to change mirrors and beam dimensions at will. Figure 5.(a) shows a simulation where an elliptic Gaussian beam with a cross-section area of $\pi \times 5 \times 50\,mm^2$ is incident at the center of a rectangular dielectric mirror with dimensions $200\,mm \times 100\,mm$. The beam suffers about 4% reflection loss. On the other hand, when the dimensions of the rectangular mirror were set to $200\,mm \times 160\,mm$, the effective reflection loss dropped to 0.26%. This example demonstrates that one needs to consider a rectangular mirror with a height that is at least 3 times larger than the major waist ω_b. Since the loss due to the finite height of the mirror will occur at each reflection, it is a critical design rule.

It is also necessary to calculate the effective reflectivity R_{eff} due to the finite width of the mirrors and the infinite extension of the width of the minor waist of the Gaussian beam. This loss is negligible at the inner area of the rectangular mirror but significant at the edge of the mirror where the laser beam enters the volume of interest. A similar numerical calculation (using Matlab) as was explained above, showed that when the beam center is $1.1\omega_a$ away from the edge of a mirror, the power loss is about 0.86%.

The closer the entering beam would be to the edge of the front mirror, the smaller angle of incidence could be achieved. A small angle of incidence will result in a dense filling of the volume between the two mirrors by the reflected beams, which is a desired feature. However, the closer the elliptic beam is to the edge of the front mirror, a larger loss will occur due to blocking by the back side of the front mirror. The beam that enters the two parallel mirrors will have a loss from the back of the front mirror, from the edge of the rear mirror and from the edge at the reflective side of the front mirror. This happens only three times at the entrance and two times at the exit from the volume. It is important to track this 'entrance' and 'exit' losses. It boils down to selecting an angle of entrance so that it would generate an optimal fill of the volume of interest with adequate optical power while minimizing 'entrance' and 'exit' loss. The numerical simulations showed that if the laser beam is a distance of $1.1\omega_a$ from the edge of the front mirror; and $1.1\omega_a$ from the edge of the reflective rear mirror, the effective reflectivity would be 0.9926%. It gives about 3% 'entrance' loss and 2% 'exit' loss.

When $1.1\omega_a$ is taken to be the edge distance, the angle of incident of the laser beam θ_i upon the mirrors can be evaluated from $\tan\theta_i = 1.5\frac{\omega_a}{d}$. Where d is the distance between the two mirrors. This relation can be used to evaluate the required width of the mirrors for a given minor waist of the elliptic Gaussian beam. The width of the mirror should equal an integral number of $1.5\frac{\omega_a}{\cos\theta_i}$. Practically, it is more convenient to use

mirrors with a given width and then adjust the distance d between the mirrors so that the beams entrance and exit into the volume will be at a small angle of incidence θ_i and with minimal reflection losses at the edges.

Figure 6.(a) shows a side view (in an x-y plane) of the field of the optical intensity on the reflective surface of one rectangular mirror. The green rectangle marks an area of 100 mm by and 200 mm. The equidistant spacing between two reflected beams is $2.2\omega_a$ at the mirror surface. This distance falls the closer one gets toward the opposite mirror (where the beams overlap). Figure 6.(b) shows a side view of the approximated field of the optical intensity at the midpoint between the two mirrors. The equidistant between the nearly parallel beams is $6\,mm$. The green rectangle mark the area where there is adequate optical density (recall that the average intensity of the laser is 2 times the required power density). A top view on the field gives a better insight into the power density field between the two mirrors. Figure 7 is a top view of the intensity field. It demonstrate the field at the x-z plane when y=80 mm.

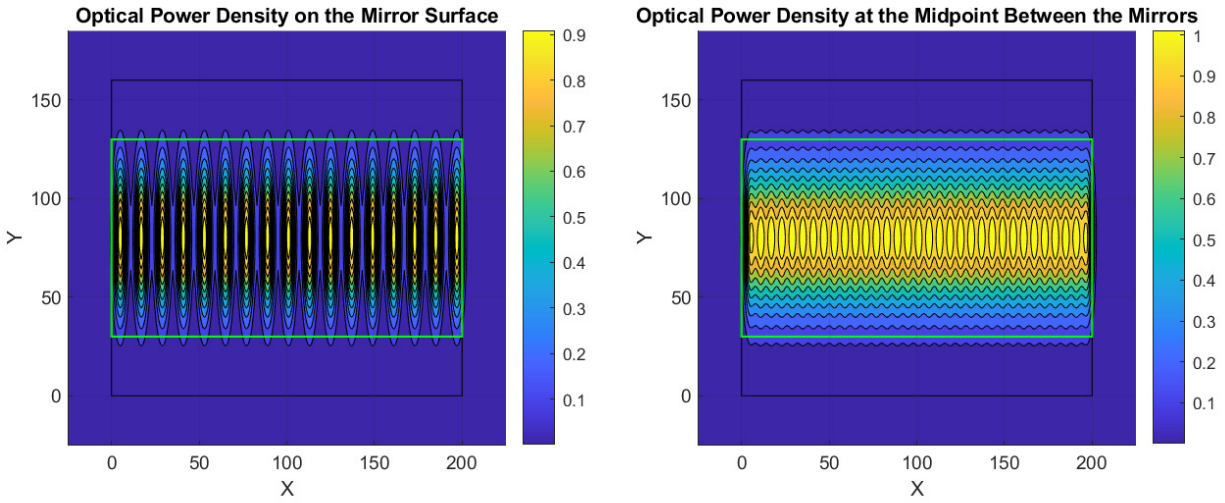

(a) (b)

Figure 6: (a) shows a side view of the field of the optical intensity on the surface of the mirrors. The green rectangular represents the mirror surface. The equidistant between reflected beams is $12\,mm$ at the mirror surface. (b) shows a side view of the field of the optical intensity at the midpoint between the two mirrors. The green rectangular marks an area of 100 mm by and 200 mm. The equidistant between the nearly parallel beams is $6\,mm$

The two mirrors are parallel but they oppose each other with a slight off-set. The off-set facilitates a minimum angle of incidence θ_i while keeping the entering beam a distance $1.1\omega_a$ from the mirror edges. I.e. the equidistant between reflected beams is $2.2\omega_a$ at the mirrors surface. The field of the optical power density is seen to be suitable for generating a sufficient signal over a large volume. The angular propagation of the Gaussian beam was achieved by rotation of the Cartesian coordinates system according to $x \rightarrow x\cos(\theta_i) + y\sin(\theta_i)$.

It is apparent that there are volumes where the power density is larger than $SNR = 20$ (due to overlapping) and volumes where the power density is bellow the level required for imaging with $SNR = 10$. Present algorithms of volumetric 3D-PTV can handle such variations. By reflecting the exiting beam backward with a slight angle, the power variations can be decreased.

Figure 8 shows the experimental set-up that was built in order to investigate multi-reflections: A continuous wave laser (CNI dragon laser) was used, two aluminium coated mirrors (height 100 mm and 150 mm width) which are 800 mm apart. The translator at the front mirror, allows to control the offset between the two mirrors. The mirrors are attached to a rail, so that their separation distance can be easily adjusted. This systems confirmed our model. Replacing the silver coated mirrors with dielectric mirrors would generate a volume with similar features to those in the simulations.

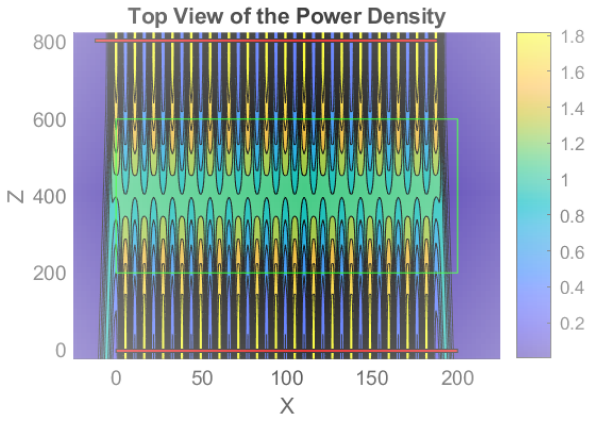

Figure 7: A top view (x-z plane,y=80 mm) of the optical intensity in the volume between the two parallel mirrors.

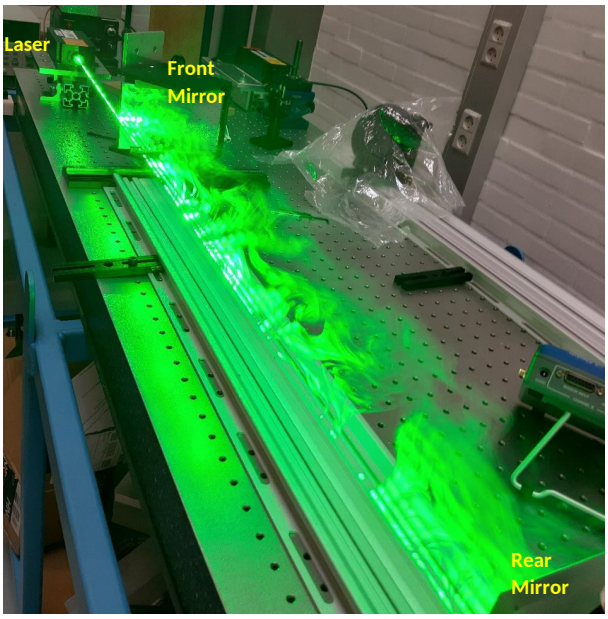

Figure 8: The experimental set-up: a laser source pass by the front rectangular mirror towards the rear mirror. It is reflected from the rear mirror towards the front mirror then back to the front mirror and vice versa.

3 Acuosto-Optic Scanning with Off-Axis Parabolic Mirror

Laser scanning PIV was first demonstrated by Brücker and Althaus (1992) and Brücker (1995) where phenomena with flow velocities of single $\frac{cm}{s}$ were measured. In those early reports, a laser sheet was scanned over a volume in a time of about $0.75s$. The relatively large time scale of the volume scan in those experiments limited the application of laser scanning to phenomena with slow velocities or to phenomena within a small volume. Since then, laser scanning advanced: velocities improved and more cameras were added to obtain more accurate tomographic analysis of the volume flow. Sun and C.Brücker (2016) measured rotational flow fields where the full volume scan was done in $8\,ms$ (10 scans per volume) and three cameras were used for tomographic reconstruction of the volumetric flow.

Scanning PIV measurements are usually done by mechanical scanning devices (rotating mirror or galvanic mirrors). The mechanical nature of a rotating mirror has the advantage of having a large angular deflection at the cost of relatively low angular-velocity and compromised repeatability due to inertia. As one aspires to increase the scanning volume, another challenge appears: the laser beam is rotated about a fixed rotation axis and pointed towards a large cylindrical lens. The limited size of commercial cylindrical lenses and spherical aberration means that only a small scanning angle can be used for transmittance of parallel beams. Here, we investigated the feasibility for using an AOM for volumetric PTV. An AOM is made of a piezoelectric crystal that is electrically induced to vibrate (Fig.9.(a)).The piezoelectric crystal is coupled to an optically transparent crystal that transmits the acoustic vibrations generated by the piezoelectric crystal (Quartz is a transparent crystal that is commonly used for deflecting lasers in the visible band). Physically, the acoustic wave that passes through the optical crystal is made of planes of high and low densities of the crystal's atoms. These planes scatter the incoming laser beam. Bragg angles are the direction (angles) where the scattering interfere constructively. These angles are given by $\theta_B = \sin^{-1}(m\frac{\lambda}{2\Lambda})$ known as Bragg equation, where θ_B is the Bragg diffraction angle, λ is the laser wavelength, Λ is the acoustic wavelength, and m is an integer denoting the order of the diffraction.

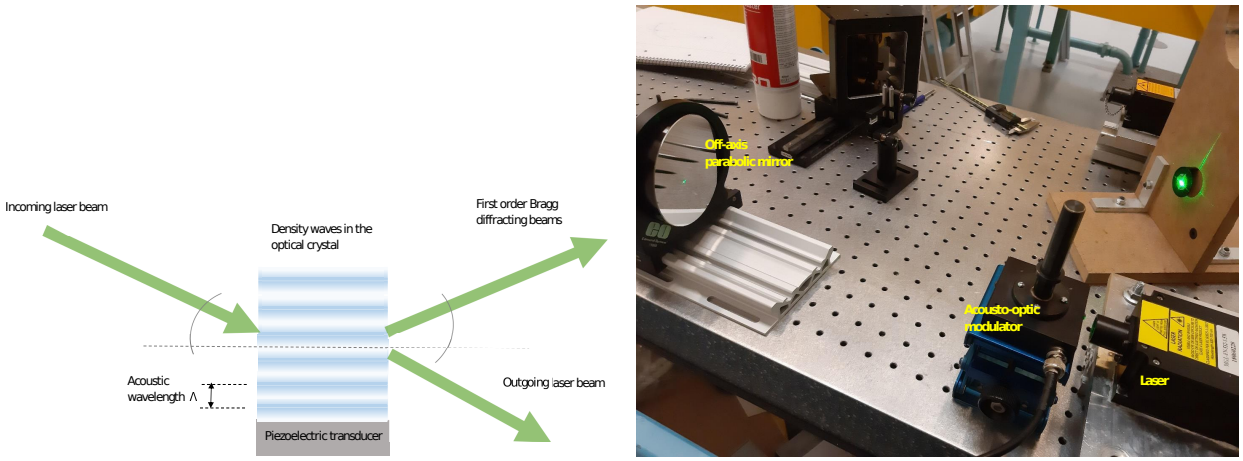

Figure 9: (a) illustrates the principle of Bragg diffraction from an AOM. (b) shows the experimental set-up of laser beam scanning by an AOM. The exit aperture of the AOM is placed at the focal point of the off-axis parabolic mirror

The experimental set-up consists of a 532 nm laser source (CNI dragon), an AOM (coherent model 305) and an off axis parabolic mirror. The laser beam enters the AOM. The exit aperture of the AOM was placed at the focal point ($f = 306\,mm$) of a $101\,mm$ diameter off-axis (30°) parabolic mirror (aluminium coated) from Edmund Optics as is shown in Figure 9.(b).

The AOM is controlled by a driver (Isomet model no.2211A-2). Both AOM and the AOM driver are outdated components. Their technical specs and manuals could not be obtained from the manufacturers. However we managed to operate them (not optimally), and characterise their operation and appreciate the potential of using an AOM. We measured the Bragg angle of the first order by measuring the distance between the zero order to the first order to be $8\,mm$ at a distance of $1450\,mm$. This means that our AOM has a deflection angle of $5.4\,millirads$. The focal length of the off-axis parabolic mirror is $306\,mm$. It gives a

beam scanned over 1.68 *mm*. This is not much, but it was useful enough to observe that the scanned beam was reflected by the off-axis parabolic mirror in parallel motion. The power efficiency was measured to be 32%. I.e. only 32% of the initial power was deflected.

In this experiment we managed to conduct only feasibility tests. The results convinced us that there is a potential in using AOM with off-axis parabolic mirror for effective volumetric PTV (or just 2D PTV).

4 Summary and Outlook

The strategy behind the two techniques presented in this report is to reuse a collimated beam by reflections (multi-reflection between two parallel mirrors) or by fast transverse shifting of the beam (laser scanning with an off-axis parabolic mirror). When the pulse energy is limited, it is an ideal approach to extend the volume of the measurement.

Our simulations and experiments suggests that multi-reflections between two reflecting mirrors is a promising technique. It can facilitate large volumetric PTV (up to $10^4\ cm^3$) with a collimated laser beam with few single *mJ* pulse energy. The only drawback of this technique is that it requires periodical cleaning of the mirrors surfaces.

The experiments for laser scanning with AOM and off-axis parabolic mirror had also shown promising results. Although, the scanned volume seems limited in the present experiment, this volume can be greatly increased by optical methods. For example, by using an off-axis mirror with larger focal length and adding 45° reflectors. Modern AOM has about 40 times max scanning angle compared with the AOM we tested, and angular velocity at sub microsecond rate. The authors believe that computerized and programmed control of the position of parallel beams from AOM with sub microsecond speeds, could lead to development of more flexible and elaborated 2D and 3D PTV techniques.

Acknowledgements

Financial support from the Poul Due Jensen Foundation (Grundfos Foundation) for this research is gratefully acknowledged.

References

Barros DC, Duan Y, Troolin DR, and Longmire EK (2021) Air-filled soap bubbles for volumetric velocity measurements. *Experiments in Fluids* 36:933–947

Brücker C (1995) Digital-particle-image-velocimetry (dpiv) in a scanning light-sheet: 3d starting flow around a short cylinder. *Experiments in Fluids* 19:255–263

Brücker C and Althaus W (1992) Study of vortex breakdown by particle tracking velocity (ptv). *Experiments in Fluids* 13:339–349

Elsinga GE, Scarano F, and B Wieneke BWvO (2006) Tomographic particle image velocimetry. *Experiments in Fluids* 13:933–947

Ghaemi S and Scarano F (2010) Multi-pass light amplification for tomographic particle image velocimetry applications. *Meas Sci Technol* 21:339–349

Hawkes J and Latimer I (1995) *Lasers Theory and practice*. Prentice Hall

Schanz D, Gesemann1 S, and Schröder A (2016) Shake-the-box: Lagrangian particle tracking at high particle image densities. *Experiments in Fluids* 70:1–27

Sun Z and CBrücker (2016) Investigation of the vortex ring transition using scanning tomographic piv. *Experiments in Fluids* 58:1–12

Zhang Y, Abitan H, Ribergård SL, and Velte CM (2021) A novel volumetric velocity measurement method for small seeding tracers in large volumes. in *14th International Symposium on Particle Image Velocimetry - PIV21, Chicago, Illinois, USA, August 1-4*